### Title

Behavioral encoding across timescales by region-specific dopamine dynamics.




### Journal

Proceedings of the National Academy of Sciences of USA, 120(7)



### Authors

Jørgensen, Søren
Ejdrup, Aske
Lycas, Matthew
et al.



### Publication Date

2023-02-14

### DOI

10.1073/pnas.2215230120

Peer reviewed

PNAS RESEARCH ARTICLE | NEUROSCIENCE

# Behavioral encoding across timescales by region-specific dopamine dynamics

Søren H. Jørgensen[a,1], Aske L. Ejdrup[a,1], Matthew D. Lycas[a], Leonie P. Posselt[a], Kenneth L. Madsen[a], Lin Tian[b], Jakob K. Dreyer[c], Freja Herborg[a], Andreas T. Sørensen[a], and Ulrik Gether[a,2]

Edited by Anders Björklund, Lund University, Lund, Sweden; received September 13, 2022; accepted January 3, 2023

**The dorsal (DS) and ventral striatum (VS) receive dopaminergic projections that control motor functions and reward-related behavior. It remains poorly understood how dopamine release dynamics across different temporal scales in these regions are coupled to behavioral outcomes. Here, we employ the dopamine sensor dLight1.3b together with multiregion fiber photometry and machine learning-based analysis to decode dopamine dynamics across the striatum during self-paced exploratory behavior in mice. Our data show a striking coordination of rapidly fluctuating signal in the DS, carrying information across dopamine levels, with a slower signal in the VS, consisting mainly of slow-paced transients. Importantly, these release dynamics correlated with discrete behavioral motifs, such as turns, running, and grooming on a subsecond-to-minute time scale. Disruption of dopamine dynamics with cocaine caused randomization of action selection sequencing and disturbance of DS–VS coordination. The data suggest that distinct dopamine dynamics of DS and VS jointly encode behavioral sequences during unconstrained activity with DS modulating the stringing together of actions and VS the signal to initiate and sustain the selected action.**

dopamine release | dopamine sensors | cocaine | mouse behavior | machine learning

## Significance

New genetically encoded dopamine sensors offer unprecedented temporal resolution for measurement of dopamine release dynamics across different brain regions over extended periods. In this study, we use the dopamine sensor dLight1.3b to decipher the role of dopamine release dynamics in the dorsal (DS) and ventral striatum (VS) of mice during simple, self-paced exploratory behavior. By AI-based splitting of behavioral kinematics into individual motifs, we link differential but highly cooperative dopamine release dynamics of DS and VS with movements on a subsecond-to-minutes time scales. In addition to coupling region-specific dopamine dynamics to behavioral sequences, our study demonstrates the strength of a machine learning-based data analysis pipeline that can be readily applied to other neurotransmitters for which genetically encoded biosensors are available.

It is essential to our survival that we can learn from experience and effectively select and sculpt our actions. By regulating reinforcement learning and movements, dopamine (DA) plays a fundamental role in this process (1–6). Interestingly, DA neurotransmission differs substantially from the classical fast synaptic transmission, as DA is a modulatory neurotransmitter exerting its effects largely via volume transmission (7, 8). DA is to a large extent released from nonsynaptic varicosities to act on extrasynaptic metabotropic receptors situated on target neurons that can be micrometers away (9). Nevertheless, DA is believed to control a plethora of physiological functions with high precision across a broad range of temporal scales (9).

The dorsal (DS) and ventral striatum (VS) constitute major target areas for dopaminergic neurons. DS is heavily innervated by projections from substantia nigra pars compacta (SNc), while VS, including the nucleus accumbens, is innervated by the ventral tegmental area (VTA) (2, 5). Numerous studies have supported that DA DS projections predominantly play a role in locomotor control, while DA VS projections mainly have been implicated in reward-related behavior (2, 4, 5, 10–15). It is well established that dysfunction of the DA system has a major impact on striatal function and contributes to a range of disorders. Loss of nigrostriatal projections, together with impairment of motor functions, is a hallmark of Parkinson's disease, while altered function of the VTA projections is thought to contribute to neuropsychiatric diseases like schizophrenia, depression, and addiction (16–18).

Several methods have been used to study the firing and release patterns of DA neurons, such as fast-scan cyclic voltammetry (FSCV), microdialysis, and electrophysiology (19–21). These techniques have revealed important functional characteristics of DA neurons, including "tonic" pacemaker-like firing and its "phasic" counterpart with trains of rapid depolarizations coordinated across neurons (3, 22–24). In response to unpredicted events, these phasic trains drive DA release on a subsecond-to-second time scale and is the putative driver behind reward-based learning. In contrast, it has been a widely held belief that motor function is modulated by slowly changing tonic activity on a time scale of tens of seconds to minutes (3). However, recent single-unit recordings of nigrostriatal neurons have suggested that movement on a much faster time scale correlates with DA neuronal firing activity (25, 26). Similarly, measurements of $Ca^{2+}$-activity in DA neurons support that subsecond changes in the activity of DA neurons may be important for triggering initiation of movement and possibly govern both future vigor and motor skill performance (11, 14, 27, 28). It is nevertheless largely unknown how these changes in neuronal activity are reflected in terminal DA release dynamics across various temporal and spatial scales in

Competing interest statement: The authors have stock ownership to disclose, L.T. has ownership interests (stock, stock options, royalty, receipt of intellectual property rights/patent holder, excluding diversified mutual funds) and is a co-founder of Seven Biosciences. The other authors declare no competing interests.

This article is a PNAS Direct Submission.



[1]S.H.J. and A.L.E. contributed equally to this work.

[2]To whom correspondence may be addressed. Email: gether@sund.ku.dk.

This article contains supporting information online at https://www.pnas.org/lookup/suppl/doi:10.1073/pnas.2215230120/-/DCSupplemental.

Published February 7, 2023.

striatal subregions, and how these dynamics are linked to discrete behavioral outcomes during unconstrained activity in animals.

To address these questions, we set out to exploit recently developed genetically encoded biosensors for DA, representing an in vivo recording modality that enables real-time measurements of extracellular DA dynamics with millisecond temporal resolution over extended periods (29, 30). Using multiregion fiber photometry recording of dLight1.3b fluorescence, we investigate fast extracellular DA dynamics concurrently in DS and VS during self-paced exploratory activity. By employing extensive data analysis together with unsupervised machine learning algorithms, we stratify mouse behavioral kinematics into individual syllables that are further correlated across time scales with the highly distinct DA dynamics that we identify in the two regions. In summary, our data suggest that distinct DA dynamics of the DS and VS jointly orchestrate behavioral structure during spontaneous activity of the mice with a DS signal that modulates the stringing together of actions and a VS signal that provides the drive to initiate and sustain the action.

## Results

**Differential DA Dynamics in DS and VS.** To assess striatal DA dynamics in freely moving mice, we injected adeno-associated virus (AAV) encoding dLight1.3b (29) under control of the human synapsin promoter (AAV9-hSyn-dLight1.3b) in the right DS and left VS of tyrosine hydroxylase male (TH) Cre mice. The mice were also injected in the VTA with an AAV encoding Cre-dependent Gi-coupled DREADD (designer receptor exclusively activated by designer drugs, AAV8-hSyn-DIO-hM4Di-mCherry) to enable later chemogenetic inhibition of VTA DA neurons (*SI Appendix*, Fig. S1*A*). At least three weeks after surgery, we recorded dLight1.3b fluorescence via implanted optical fibers as a proxy for extracellular DA dynamics in the mice during self-paced unconstrained activity in an open-field arena (Fig. 1 *A* and *B* and *SI Appendix*, Fig. S1 *B* and *C* for calculation of zF). DS displayed incessant rapid fluctuations, while VS showed slower and longer lasting fluctuations (Fig. 1*B*). These signals were interchangeable across hemispheres when sensor and fibers were shifted to left DS and right VS (*SI Appendix*, Fig. S1*D*). Note that these mice were not injected with AAV8-hSyn-DIO-hM4Di-mCherry into VTA, yet we still saw the same difference between DS and VS. Moreover, we observed no difference between the signal and isosbestic channel when mice were injected with GFP (AAV9-hSyn-EGFP-WPREpA) (*SI Appendix*, Fig. S1*E*) and found that the differences between DS and VS were patch cord fiber-independent (*SI Appendix*, Fig. S2 *A* and *B*). Indeed, previous studies have also supported the strong specificity of the dLight sensors in DS and VS (see e.g., refs. 29, 31, and 32). To analyze the recorded signals in greater detail, we computed the spectral energy density of the two regions, revealing a differential distribution of activity levels across frequency bands. Most of the DS signaling occurred in the 0.1- to 10-Hz range, whereas VS showed markedly slower dynamics (Fig. 1 *C* and *D*). After photobleaching correction, DS showed minimal activity below 0.02 Hz. In contrast, VS exhibited DA fluctuations with durations upward of 30 min but displayed minimal activity faster than 1.25 Hz (Fig. 1 *C* and *D* and *SI Appendix*, Fig. S3 *A*–*C*). Due to DS tapering off at 0.01 Hz, however, we decided to arbitrarily split the signal from both regions in two domains for later data interpretation purposes; a slow domain defined as fluctuations of 0.01 Hz and below, and a rapid domain defined as anything above (Fig. 1*C* and *SI Appendix*, Fig. S3 *A* and *B*).

To further investigate the biological significance of the observed DA dynamics, we computed the first-order derivative (Δ) of each decile of the signals (Fig. 1*E*, *Top*). Plotting the mean derivative (mean ΔzF) by signal amplitude (zF percentile) revealed a steeper slope for DS compared to VS (Fig. 1*E*, *Bottom*). This is in line with a more rapidly fluctuating signal in the DS than in VS (Fig. 1*D*) and supports that DS is capable of both releasing and clearing DA more swiftly than VS as suggested previously (33). To test whether the data were in line with the tonic-to-phasic firing model of DA signaling (22, 24, 34), we simulated striatal DA dynamics based on tonic firing (2 to 10 Hz) of DA neurons. The extracellular DA level arising from release from a high number of tonically driven terminals can accurately be modeled by differential equations with a homogenous Poisson process as input (35–37). This mirrors a regular tonic activity with random phase shifts between neurons. Indeed, fluctuations are still present if DA release dynamics is simulated by such a process (Fig. 1*F*, *Top*). However, fluctuations derived from a Poisson process produce a homogenous signal, as they represent random variations in an otherwise homogeneous input (35–37). Similarly, in the tonic-to-phasic firing model of DA signaling tonic firing is a homogenous signal, whereas the informational encoding is added by phasic firing, or lack thereof, which is a heterogeneous process. A feature of a system driven by a Poisson process is the uniform variance of the first-order derivative across intensity levels (Fig. 1*F*, *Bottom*). Therefore, we computed the variance of the derivative across signal intensity for DS and VS (Fig. 1*G*), which represents a measure of heterogeneity in the release patterns. Importantly, VS dynamics matched the tonic-to-phasic firing model of DA signaling, where biological information is encoded by phasic firing giving rise to transients (6). That is, we observed no significant change in variance for the lowest half of the DA signal as compared with the bottom 10th percentile, implying that the lower intensity-ranges represent random fluctuations from such a constant Poisson process. This suggests that a basal level of DA is sustained by pacemaker activity. Signal heterogeneity only seemed to be added in the upper ranges, where the variance of the derivative was larger, and the signal was dominated by transients conceivably representing novel information encoded by changes in firing rates. The same was not true for DS. Instead, variance increased from the lowest decile throughout (Fig. 1*G*), indicating fluctuations across all DA levels are driven by different upstream input phenomena, rather than constant release from tonic firing. The concept is schematized in Fig. 1*H*.

**Exploration and Reward-Seeking Behavior Promotes Ramp-Like DA Release in VS but Not DS.** We investigated DA dynamics of DS and VS in two simple behavioral paradigms believed to implicate DA release. First, we assessed DA release correlates at entry to a novel environment by habituating mice to an open area for 15 min and then opening a gate to a small, adjacent novel chamber (Fig. 2*A* and *SI Appendix*, Fig. S4*A*). The VS signal exhibited a fast, ramp-like increase in fluorescence, beginning immediately before entry to the novel chamber and returning to baseline after ~20 s. As expected, the mice also responded to a new environment with an increase in locomotion that persisted after the increased VS DA signal had subsided (Fig. 2*B*). There was no significant change in DS at entry although the average signal across mice indicated a timing of transients (Fig. 2*A* and *SI Appendix*, Fig. S4*C*). There was, however, a correlation between locomotion in the novel area and the DA response for both DS and VS supporting a role of the DA signal in coding of movement velocity (*SI Appendix*, Fig. S4*D*). The gate to the novel chamber was closed after 5 min, and the mice were left in the "old" arena for 30 min. We subsequently placed female-soiled bedding, known to be a source of intrinsically rewarding pheromones (38), in a second adjacent chamber and opened the gate (Fig. 2*C*). As the mice approached the bedding,

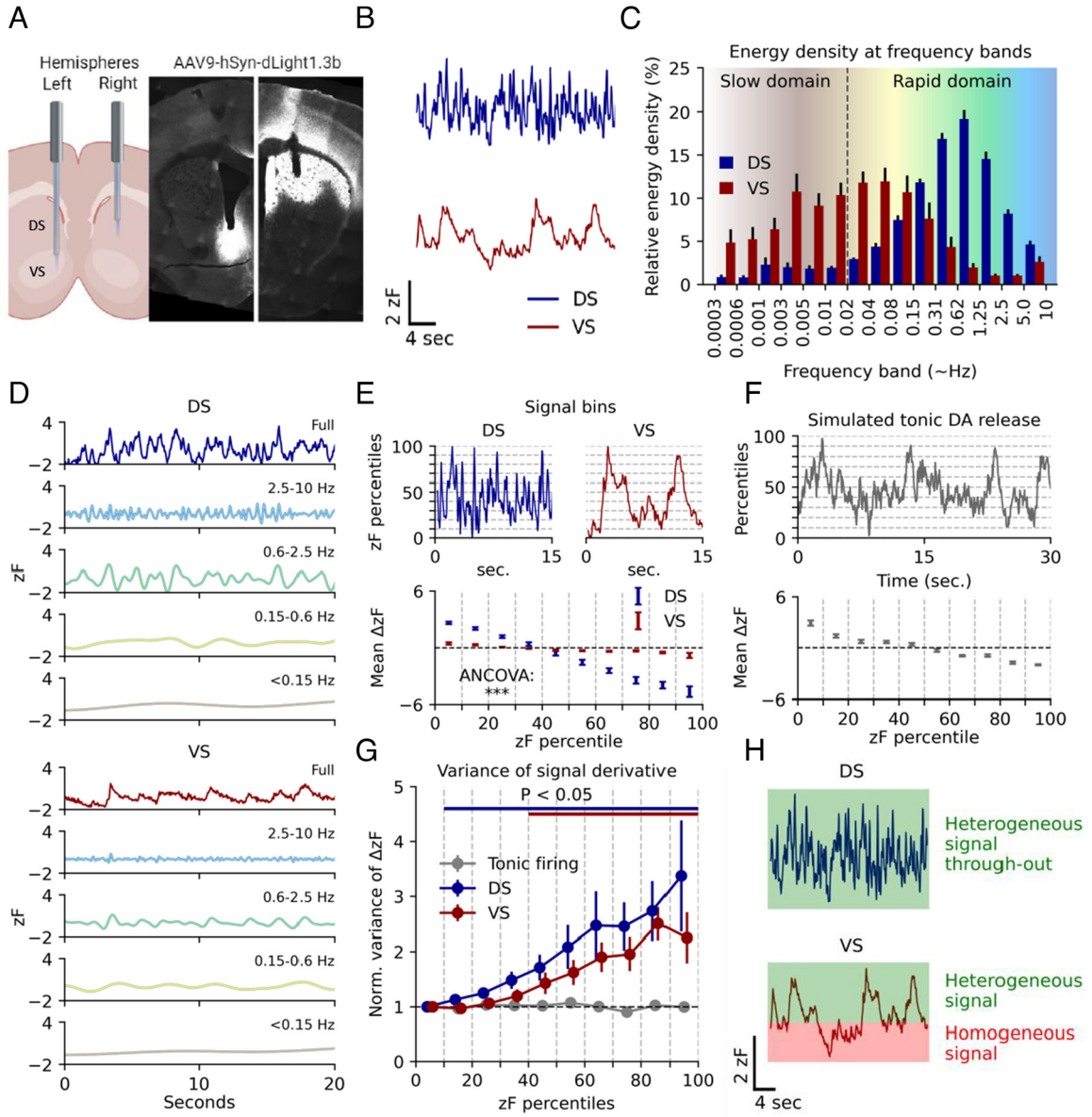


**Fig. 1.** Basal DA dynamics differ between DS and VS during self-paced exploratory activity. (*A*) Injection of AAV9-hSyn-dLight1.3b in the right DS and left VS of Th-Cre mice followed by implantation of 200-µm optical fibers. Histology on coronal sections of the striatum show dLight1.3b expression and fiber location. (*B*) Representative traces from right hemisphere DS and left hemisphere VS DA fluctuations as assessed by dLight1.3b fluorescence measured during self-paced exploratory activity in an open-field arena that the mice had been exposed to two to three times before. (*C*) Spectral energy density of the two regions by frequency band. Error bars indicate SEM, n = 8 mice. (*D*) Representative frequency domains for DS and VS isolated by multiresolution analysis of the maximal overlap discrete wavelet transform. Colors match the corresponding domain in (*C*). (*E*) *Top*: Representative traces of VS and DS split into percentile bins of 10 across fluorescence amplitudes. *Bottom*: First-order derivative for each percentile bin of fluorescence amplitude for both regions. Error bars indicate SEM, n = 8 mice, ANCOVA, region:percentiles, F = 1,199.5, *P* = 1.8E-16). (*F*) *Top*: Poisson-driven tonic DA simulation. Fluctuations are present despite the temporally uniform process. Dashed lines indicate amplitude percentiles. *Bottom*: First-order derivative for each percentile bin of fluorescence amplitude. Error bars indicate SEM, n = 10 simulations. (*G*) Variance of the first-order derivative for each percentile bin normalized to bottom 10th percentile for simulated tonic release and DS and VS measurements. Error bars indicate SEM, *P* < 0.05 indicated by bars matching region color, Student's *t* test, $H_0 = 1$, multiple comparisons corrected for each percentile with the Benjamini–Hochberg procedure (α = 0.05). (*H*) Conceptual Figure of interpretation of data in (*G*).

the signal in VS ramped up as a conceivable response to the odor of the bedding (Fig. 2 *C* and *D* and *SI Appendix*, Fig. S4*E*). When splitting the signal around the first encounter into frequency bands, it was clear that this signal change in VS was mainly driven by frequencies slower than 0.6 Hz (Fig. 2*E*). Although peaks of DA release in DS were observed surrounding the encounter, there were no significant changes in DS (Fig. 2 *C*–*E* and *SI Appendix*, Fig. S4 *B* and *E*). We next stimulated the inhibitory DREADD, hM4Di, that we had expressed in the VTA DA neurons of the dLight1.3b-injected mice (*SI Appendix*, Fig. S1*A*). Indeed, we have previously demonstrated that stimulation of hM4Di in VTA DA neurons reduces exploratory locomotor activity and neuronal firing activity in ex vivo slice experiments (39). Administration of the DREADD agonist CNO (clozapine N-oxide) (2 mg/kg) caused a long-lasting decrease in the slow signal of VS with no significant decrease observed for DS (*SI Appendix*, Fig. S4*F*). Note that we observed a short-lasting increase in both DS and VS immediately after injection, likely because of handling as this was also observed for vehicle (*SI Appendix*, Fig. S4*F*). Detailed analysis revealed shifts also in the rapid dynamics of VS (*SI Appendix*, Fig. S4*G*) with reduced power in the 0.1- to –2-Hz range in response to CNO (Fig. 2*I*). Furthermore, CNO reduced the magnitude of the response in VS to female bedding, while in parallel the CNO-treated mice spent more time closing the distance to the

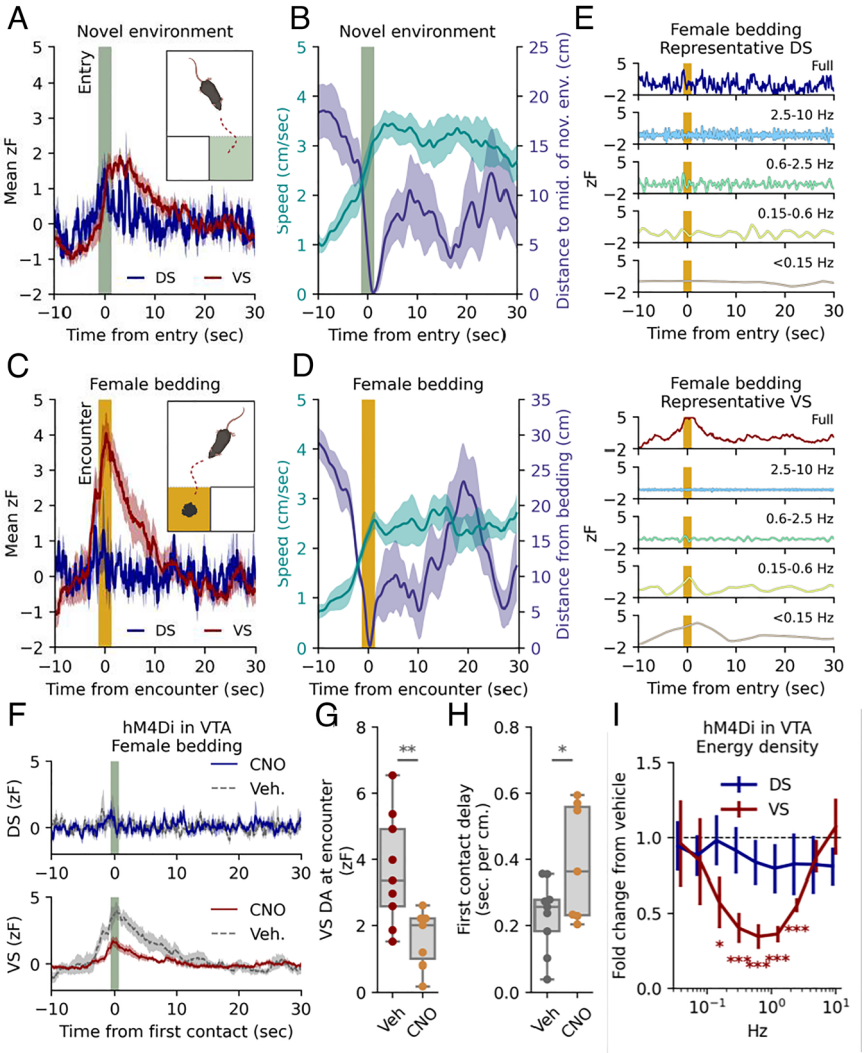


**Fig. 2.** Exploration and reward-seeking behavior promotes ramp-like DA release in VS but not DS, which can be blunted by chemogenetic Gi-stimulation of VTA DA neurons. (*A*) Mean DA traces for right DS and left VS for TH-Cre mice expressing dLight1.3b in the right DS and left VS, and AAV-hSyn-DIO-hM4Di-mCherry in VTA. The traces are time-locked to entry into a novel chamber (t = 0, dark green band). The shaded area indicates SEM, n = 9 mice (two trials included for each mouse). (*B*) Mean speed (*Left* y-axis) and distance to middle of novel chamber (*Right* y-axis). Time-locked to entry (t = 0, dark green band). The shaded area indicates SEM, n = 9. (*C*) Mean fluorescent DA traces for right DS and left VS time-locked to first encounter with female-soiled bedding (t = 0, orange band). The shaded area indicates SEM, n= 9. (*D*) Mean speed (*Left* y-axis) and distance to female bedding (*Right* y-axis). Time-locked to first encounter (t = 0, orange band). The shaded area indicates SEM, n = 9. (*E*) DS (*Top*) and VS (*Bottom*) signals split into representative frequency domains isolated by multiresolution analysis of the maximal overlap discrete wavelet transform. Time-locked to first encounter with female-soiled bedding (t = 0, orange band). Colors match the corresponding domain in Fig. 1*C*. (*F*) Response to female bedding as in (*C*). after i.p. injection of either vehicle or 2 mg/kg CNO; DS (dark blue, *Top*) and VS (dark red, *Bottom*) signals are plotted for both vehicle (dashed line) and CNO (solid line). Shaded area indicates SEM, n = 9 for both groups). (*G*) Box plot of DA levels in VS at first encounter (***P* = 0.009, unpaired student's *t* test, n = 9). (*H*) Box plot of delay from gate removed to first encounter: unit is s/cm to account for differences in starting position for individual mice (**P* = 0.04, unpaired Student's *t* test, n = 9). (*I*) Change in spectral energy density from vehicle to CNO for minutes 15 to 30. Error bars indicate SEM, n = 9, Student's *t* test, $H_0 = 1$, FWER correction for all nine frequency bands with the Bonferroni–Holm method, **P* < 0.05, ***, *P* < 0.001.

bedding (Fig. 2 *F*–*H*). Summarized, the data support the central importance of the VTA DA neurons for both slow and fast DA dynamics in VS and are consistent with the role of VS DA in reward-seeking behavior. We also expressed hM4Di in DA SNc neurons but detected no effect of CNO administration on the DA signal for neither DS nor VS despite histological confirmation of expression (*SI Appendix*, Fig. S4*H*). We have no immediate explanation for this observation but speculate that it relates to the previously reported higher D2 auto-receptor expression and stimulation in nigrostriatal SNc neurons as compared with VTA neurons, leading to saturated Gi-stimulation (40, 41).

**DA Release in DS and VS Correlates with Action Selection on a Subsecond and Minute-to-Minute scale.** The activity of D1R and D2R-expressing medium spiny neurons (MSNs) of the direct and indirect pathways, respectively, were recently shown to encode behavior within the DS by organizing moment-to-moment action selection with subsecond precision (42). An unresolved question is how this may be modulated by input from DA projections. We thus sought to determine how individual behavioral motifs, referred to as syllables (i.e., run, walk, turn etc.), might be encoded by DA release in DS and VS. Top-down video tracking of the behavior was analyzed, using DeepLabCut (43) (Fig. 3*A*). Limb trajectories were tracked, segmented into individual syllables using the unsupervised clustering algorithm B-SOiD (44), and aligned with simultaneously recorded dLight1.3b DA traces (Fig. 3 *A* and *B*). The clustering algorithm identified >50 unique syllables; however, a low usage and high intermouse variability was seen for the less frequent (*SI Appendix*, Fig. S5*A*), and consequently we focused on the twenty most recurring syllables (Fig. 3*C*). We computed the average DA

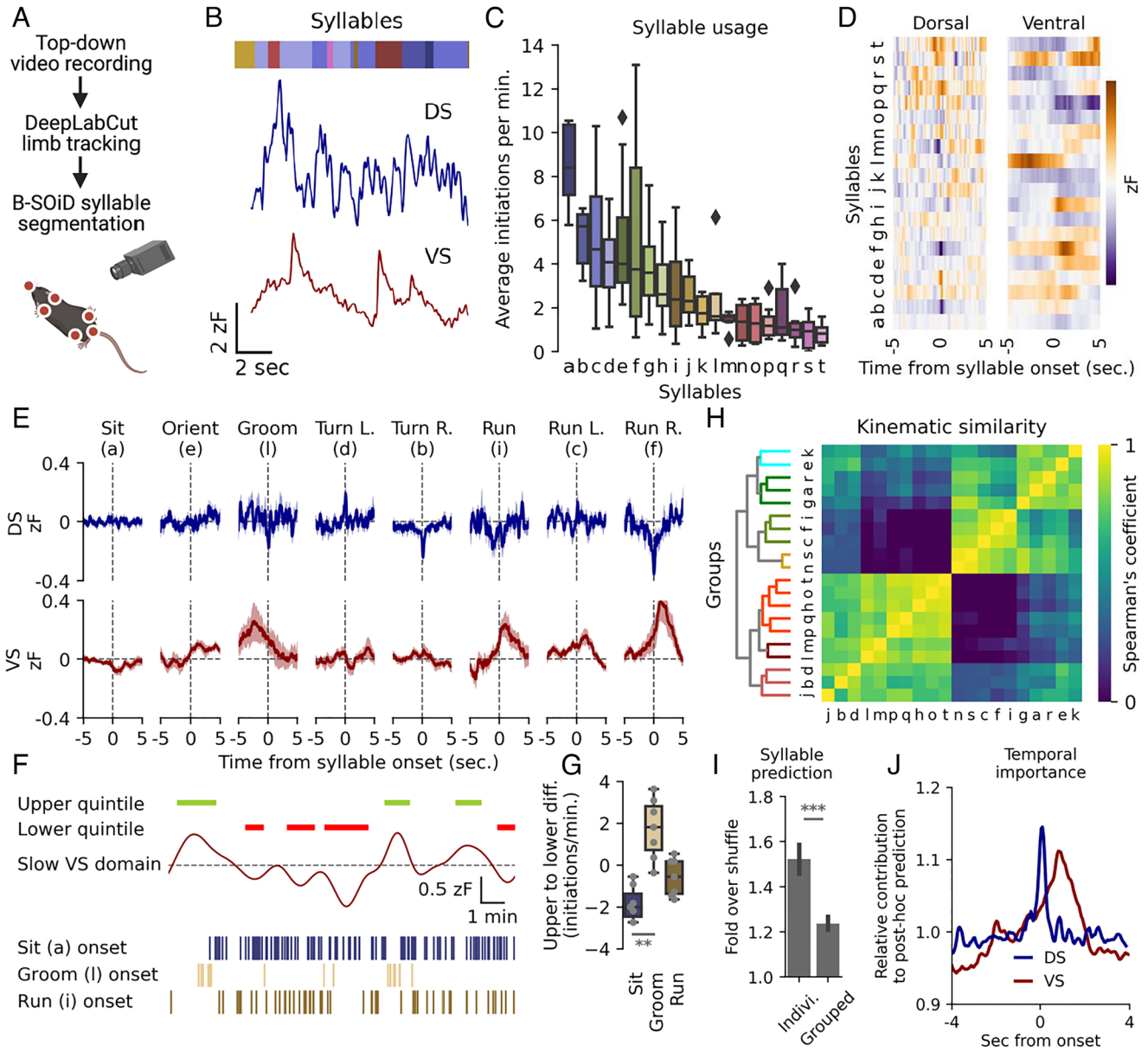


**Fig. 3.** DS and VS DA dynamics correlate with movement across timescales. (*A*) Syllable identification pipeline. Mice were filmed from above, limbs tracked with DeepLabCut (43), and syllables segmented with an unsupervised clustering algorithm, B-SOiD (44). (*B*) Identified syllables (colored bar, each color representing a syllable) aligned to the DA signals in both regions. (*C*) Box plots of frequency of initiation for 20 most frequent syllables, n = 9. Syllables assigned letters in descending order. Black diamonds indicate outliers. (*D*) Average DA trace around onset in both DS and VS for each of the 20 most frequent syllables. (*E*) Fluorescent DA trace of DS (blue) and VS (red) around onset for eight humanly unambiguous syllables. The shaded area indicates SEM, n = 9. (*F*) Representative example showing frequency of sit (blue), groom (sand) and run (brown) correlated with slow DA oscillations in VS. Green bars indicate periods of upper quintile and red bars lower quintile. Syllable onsets are depicted with lines below. (*G*) Box plot of difference in frequency for upper and lower quintiles of slow VS levels (one-way ANOVA for all eight syllables in (*E*), F = 3.5, $^{**}P$ = 0.004. Post hoc Tukey HSD: sit = groom, $^{**}P$ = 0.01, n = 9, see *SI Appendix*Fig. S6*A* for statistics all eight syllables). (*H*) Syllables hierarchically clustered by prediction certainty with the Spearman correlation coefficient and segmented into seven differently colored groups by arbitrary threshold (see *SI Appendix*Fig. S5*C* for human annotations). (*I*) A random forest classifier correctly predicts individual syllables at a higher rate than kinematically grouped syllables when compared to shuffled guessing (fold over shuffle ± SEM, $^{***}P$ = 5.2E-12, paired, two-tailed student's *t* test, n = 9, 20 train-test iterations). (*J*) Relative contribution to classifier prediction by region (DS, blue. VS, red) around onset of syllables (n = 9, 20 train-test iterations).

trace at onset for each syllable from all identified instances in both regions (Fig. 3*D*). For several syllables we observed a distinct pattern in the averaged DA signal surrounding onset that differed between the two striatal regions. For DS, the general picture observed was fluctuations that peaked positively or negatively right at syllable onset. VS activity was also primarily fixed around syllable onset but changes were more gradual and longer lasting (Fig. 3*D* and *SI Appendix*, Fig. S5 *B* and *C*).

Eight syllables could unambiguously be classified by human observers, and the patterns of DA signal around onset are shown in Fig. 3*E* (see *SI Appendix*, Fig. S5*B* for all syllables). For two stationary syllables, sit and groom, we observed no detectable correlation to DS fluctuations. However, for grooming a distinct pattern emerged in VS with a transient increase in the signal peaking immediately before syllable onset, suggesting that the action either requires or promotes DA release. For turns, we observed mirrored DA activity for opposite turn directions. Ipsiversive (right) turns correlated with a brief depression at onset and contraversive (left) turns with a brief elevation in DA signal in right DS (Fig. 3*E*). Note that by expressing dLight1.3b and implanting fibers in the opposite hemispheres, we observed an identical mirrored pattern (*SI Appendix*, Fig. S6*A*). For run initiation, the most

prominent feature was elevated DA levels in VS with no clear pattern for DS (Fig. 3*E*). Curiously, during running turns, we observed a pattern akin to the rise during a run in VS, accompanied by the DS pattern of a stationary turn, suggesting a modular design of at least some of the identified syllables (Fig. 3*E*). Note that as B-SOiD segments syllables at 100-ms resolution, peak activity timing during turns could not be temporally distinguished from onset (*SI Appendix*, Fig. S6*B*).

While the DS signal showed minimal minute-to-minute fluctuations, such slow fluctuations were present in VS (Fig. 1*C* and *SI Appendix*, Fig. S3 *B* and *C*). Intriguingly, these slow fluctuations correlated with the propensity of using distinct syllables. Sitting was significantly more frequent during the bottom quintile of these slow fluctuations as compared with the top quintile, while grooming demonstrated the opposite pattern (Fig. 3 *F* and *G* and *SI Appendix*, Fig. S6*C*). The run syllable, however, did not occur more frequently during long-term elevations, indicating a complex relationship between slow DA levels, second-to-second fluctuations, and behavioral syllables.

We subsequently tested a two-part hypothesis; the DA traces predict movements, and motions with similar kinematic correlate with similar traces. We used Spearman's correlation coefficient to cluster syllables by kinematics (Fig. 3*H*, see *SI Appendix*, Fig. S5*D* for human annotations) and we used machine learning by training a random forest classifier to predict syllables based on DA traces of both DS and VS. When predicting individual syllables, the classifier performed clearly better than chance when tested on a held-out data set (1.5-fold over shuffle, Fig. 3*I*) (see prediction for the eight most unambiguous syllables in *SI Appendix*, Fig. S5*E*), primarily using information at onset for DS and the seconds following for VS (Fig. 3*J*). In contrast, syllable prediction became less accurate (1.2-fold over shuffle) when predicting syllables grouped by kinematics (Fig. 3*I*). This highlights the predictive power of DS and VS DA traces when inferring behavior while also showing that movements of similar kinematics might differ substantially in their underlying DA signals.

**Cocaine Alters Rapid Dynamics and Disrupts DA Correlation to Action Selection.** Next, we investigated the effect of cocaine that inhibits DA reuptake by blockade of the dopamine transporter (DAT) (45). Cocaine (20 mg/kg i.p.) caused a substantial increase in the slow DA signal in both DS and VS, which as expected was accompanied by increased locomotor activity (Fig. 4*A*). No increase in fluorescent signal was observed in mice injected with AAV9-hSyn-EGFP-WPREpA (*SI Appendix*, Fig. S7*A*). The cocaine-induced increase in fluorescence in VS was 20 to 40 times the SD of the signal at baseline, whereas slow DS fluctuations only increased with 4 to 8 SDs (*SI Appendix*, Fig. S7*B*). As the fluorescence is measured in arbitrary units and z-scored to baseline signal in each region, amplitudes in the two regions cannot be compared directly. Therefore, these observations may suggest that cocaine increases DA in VS to a greater extent as compared with DS or, alternatively, that the absolute DA fluctuations in DS under basal conditions are of a larger magnitude as compared with VS.

The fast DA dynamics changed radically 10 to 20 min after cocaine with a shift toward lower frequency fluctuations (Fig. 4 *B* and *C* and *SI Appendix*, Fig. S7*C*). The rapid VS signal was shifted so far toward low-frequency fluctuations that it started to blend with our threshold for slow fluctuations. This shift in VS was accompanied by a slight but significant increase in energy of the fastest domain (Fig. 4*C* and *SI Appendix*, Fig. S7*C*). Computing the variance of the first derivative after vehicle resembled that found in DS and VS for untreated mice (Figs. 4 *D* and 1 *G*). In contrast, variance of the derivative changed drastically after cocaine to the point where no significant differences were observable across fluorescence intensities in DS and VS. This could suggest that the observed fluctuations after cocaine were random variations in a constant upstream process generated by a uniform input, such as tonic firing.

Analysis (as in Fig. 3) of behavioral syllables after cocaine showed a marked change in frequency of various syllables (Fig. 4*E* and *SI Appendix*, Fig. S7 *D* and *E*). Syllable usage, however, did not become more disordered. Rather, entropy of the system decreased slightly (Fig. 4*F*), likely because of more frequent locomotion initiations. We also observed changes in the average DS for several syllables with run and run left/right being characterized by a strong depression of signal in DS around initiation. In contrast, sitting correlated with an uptick in DS release, as opposed to no correlation after vehicle injection. VS, on the other hand, lost most of its correlative signatures, which might be the result of the strongly elevated slow DA levels. Interestingly, the behavioral classifier became stronger at predicting syllables from DA traces after cocaine (Fig. 4*H*). This increase in predictive power came almost exclusively from the DS trace with a broader temporal window now contributing to the predictions (*SI Appendix*, Fig. S7F).

Because variance of derivative indicated that the observed DA fluctuations after cocaine were the result of random fluctuations in a homogenous signal, and because syllable usage did not appear more disordered, the DA fluctuations of DS did not seem to encode individual syllable selection. Rather, we hypothesized that the observed correlation between DA and syllables might reflect the stringing together of actions (4). To assess this, we mapped the frequency of transition from one syllable to another (Fig. 4 *I* and *J* and *SI Appendix*, Fig. S7*G*). Interestingly, we observed that the most used transition frequencies after vehicle were down-regulated after cocaine, whereas the less frequent transitions were generally up-regulated (Fig. 4*K*). This corresponds to a decrease in transition orderliness as apparent when calculating the system entropy from the transition matrix (Fig. 4*L* and *SI Appendix*, Fig. S7*E*).

**DS and VS DA Dynamics Correlate on a Subsecond and Tens-of-Second Scale.** Finally, we wanted to determine whether DA dynamics in DS and VS overall were temporally correlated. We therefore quantified the cross-correlation of the signals by time-shifting the DS trace (Fig. 5*A*). A maximal overlap for DA signal in the two regions was observed when DS was shifted ~0.5 s forward (Fig. 5*B*), indicating that DA release in the DS is predictive of a subsequent VS release. DS continued to positively correlate with increased VS signal for up to 20 s. When shifting the DS signal backward in time, we observed a negative correlation between DS and VS release from −10 to −20 s, showing that VS release predicted a future depression in DS signaling. This correlation was spread across frequency domains, with correlations across timescales (Fig. 5*C*).

We subsequently assessed the correlation between the DS and VS signal in CNO-injected mice expressing hM4Di in VTA DA neurons. Strikingly, despite the major changes in VS dynamics (Fig. 2*J*), the peak correlation when normalized to DS autocorrelation was statistically identical to that of vehicle (Fig. 5 *D* and *E*). Thus, metabotropic inhibition of VTA neurons is not sufficient to disturb the apparent coordination between the DS and VS DA signals. A different picture, however, emerged in mice upon cocaine exposure. As with CNO, the peak correlation when normalized to DS autocorrelation was not statistically different from vehicle (Fig. 5 *D* and *E*). However, for cocaine we observed an altered lag of maximal cross-correlation after cocaine as compared to vehicle or CNO conditions with intermouse variation increasing significantly for cocaine (Fig. 5 *D* and *F*). This suggests a temporal decoupling in the cross-regional coordination of DS and

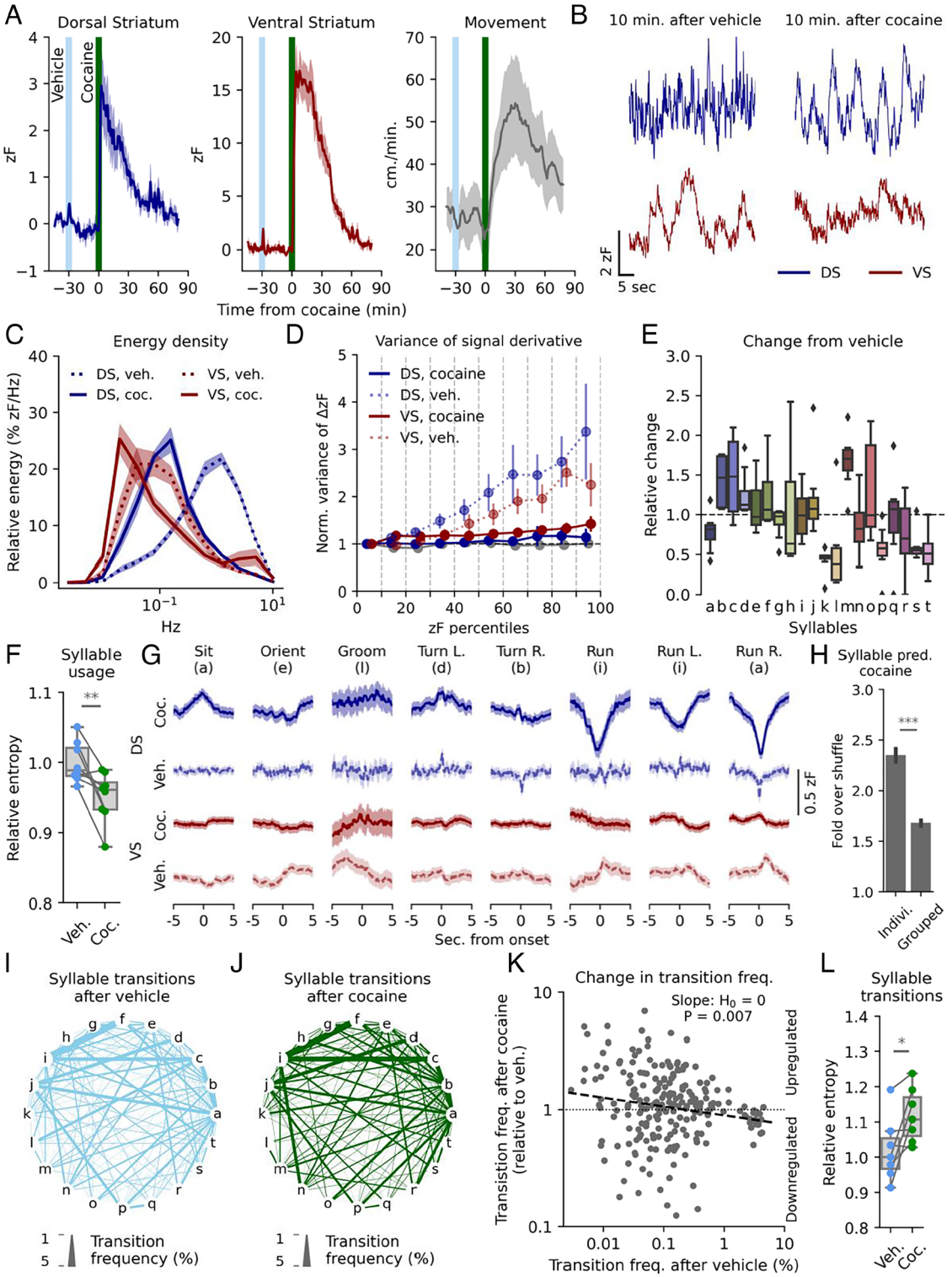


**Fig. 4.** Cocaine alters rapid DA dynamics and ablates VS correlation to sub-second movements. (*A*) dLight1.3b expressing mice were habituated to an open arena for 15 min before receiving vehicle i.p., followed by 20 mg/kg cocaine after 30 min. The signal in DS (*Left*) and VS (*Middle*) and movement (*Right*) is plotted in 1-min bins. Shaded areas indicate SEM, n = 8 mice. (*B*) Representative traces of rapid dynamics in DS and VS 10 min. after vehicle (*Left*) and cocaine (*Right*). (*C*) Spectral energy density of DS and VS signal 10 to 20 min after vehicle (dashes lines) and cocaine (solid lines). Shaded areas indicate SEM, n = 8 mice. (*D*) Variance of the first-order derivative for each percentile bin normalized to bottom 10th percentile for simulated tonic release and DS and VS measurements. Error bars indicate SEM; no percentile survived multiple comparison with the Benjamini–Hochberg procedure (α = 0.05) after cocaine (Student's *t* test, H0 = 1, n = 8). (*E*) Box plot of change in syllable frequency from vehicle to cocaine administration for the 20 most frequent syllables, n = 8 mice. (*F*) Entropy of syllable usage after vehicle (light blue) and cocaine (green). Normalized to vehicle mean (***P* = 0.009, two-sided, paired Student's *t* test, n = 8 mice). (*G*) Mean DA traces for DS (blue) and VS (red) after vehicle (dashed line) or cocaine (solid line) for eight selected syllables. Lines are averaged across mice with shaded areas indicating SEM, n = 8 mice. (*H*) A random forest classifier correctly predicts syllables 2 to 2.5 times as often as shuffled guessing and performs significantly better at individual syllables compared with kinematically similar groups (****P* = 1E-21, paired, two-tailed Student's *t* test). (*I* and *J*) State-transition plot of syllable transition frequency after vehicle (*I*) and cocaine (*J*) injection. Letters represent individual syllables with line thickness between the letters indicating transition frequency between the two syllables in absolute percentages. (*K*) Syllable transition frequencies after vehicle injection vs. transition frequency after cocaine relative to vehicle. The dashed line indicates least square linear fit (***P* = 0.007, $H_0$: slope = 0). (*L*) Entropy for the transition matrix (*SI Appendix* Fig. S7*E*) after vehicle (light blue) and cocaine (green). Normalized to vehicle mean (**P* = 0.015, one-sided, paired student's *t* test, n = 8 mice).

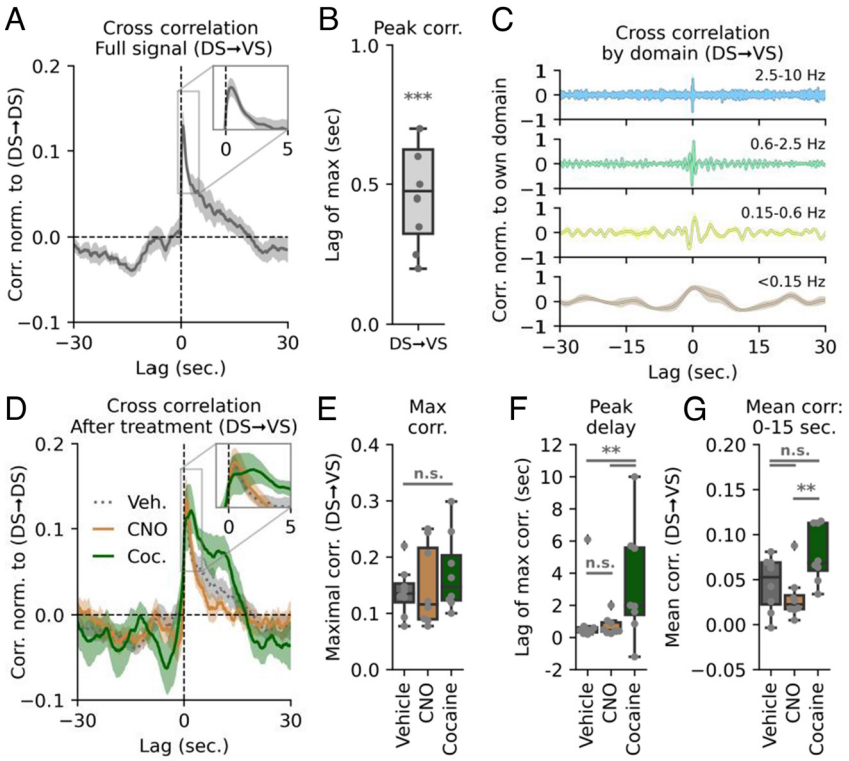


**Fig. 5.** Cocaine alters cross-correlation of intrastriatal DA activity. (*A*) DS–VS cross-correlation normalized to DS auto-correlation. The *Inset* shows correlation peak and highlights that release in the DS is predictive of a subsequent VS release with approx. 0.5-s lag time. The shaded area indicates SEM, n = 8 mice. (*B*) Box plot of lag of maximal DS–VS cross-correlation (***$P$ = 4.4E-5, one-sample Student's $t$ test, n = 8 mice). (*C*) DS–VS cross-correlation by different frequency bands. Each domain is normalized to self within each mouse. Colors correspond to frequency domains in Fig. 1*C*. (*D*) DS–VS cross-correlation for vehicle (dashed gray line), CNO (solid orange), and cocaine (solid green). Shaded area indicates SEM, n = 8 mice for all three groups. (*E*) Maximal cross-correlation remains unchanged (one-way ANOVA: F = 0.58, $P$ = 0.57, n = 8). All treatments normalized to DS auto-correlation. (*F*) Box plot of distribution of max lag in DS–VS cross-correlation for vehicle, CNO, and cocaine. Only cocaine significantly alters correlation timing (veh.:CNO, $P$ = 0.16; veh.:cocaine, **$P$ = 0.002; CNO:cocaine, **$P$ = 0.004, Levene variance test, FWER correction with Bonferroni–Holm, n = 8 mice). (*G*) Quantification of mean cross-correlation from 0 to 15 s. VS lag. Vehicle is not significantly different from the two treatments, but CNO and cocaine differs (one-way ANOVA: F = 7.56, $P$ = 0.0059, n = 8; Tukey HSD: veh.:CNO, $P$ = 0.58; veh.:cocaine, $P$ = 0.09; CNO:cocaine, **$P$ = 0.01).

VS DA release. Moreover, the DS signal correlated with the VS signal further into the future for cocaine as compared to the VTA-inhibition by CNO (Fig. 5*G*). The difference between vehicle and the two treatments, however, was not significant.

## Discussion

The striatum constitutes an essential subcortical forebrain nucleus that receives major input from midbrain dopaminergic neurons and plays a key role in motor functions and reward-related behavior (2). Here, we use the recently developed, genetically encoded DA biosensor dLight1.3b to gain insights into how extracellular DA dynamics on different time scales in striatal subregions are linked to self-paced exploratory behavioral sequences. We achieve these insights by applying several machine learning-based data algorithms that enable highly detailed dissection of fast transmitter fluctuations in relation to discrete behavioral output. Together, our data show how major differences in the extracellular DA dynamics of the mouse DS and VS might underlie distinct, yet cooperative functions, of the two regions. Indeed, previous studies have indicated region-specific activity of DA neurons when the signals were aligned with well-defined behavioral events (11, 46–48). However, there has been little focus on subregion-specific DA release dynamics over extended periods, as we measure in the present study. Interestingly, the observed difference in subregion-specific DA dynamics is not readily predicted from electrophysiological recordings of dopaminergic neuronal firing as these have reported similar overall firing rates of DA neurons in SNc and VTA (49–51). Thus, the differential DA release in substriatal regions may not be simply explained by differences in the neuronal firing rate, consistent with the recently demonstrated partial dissociation of DA release in VS from neuronal firing in the VTA (13).

Earlier studies involving primarily electrophysiological recordings and FSCV led to the classical assumption that bursts of DA release on a subsecond-to-second time scale is critical for reward-based learning, while slower changing tonic activity is critical for control of movements (3). However, recent employment of electrophysiology and genetically encoded $Ca^{2+}$ sensors to assess firing activity of DA neurons have implicated fast changes in activity in movement control (11, 14, 25–28). In the present study, we take this a step further to correlate highly differential DA fluctuations in DS and VS with discrete behavioral actions. By splitting the activity of the mice into behavioral syllables, we show that initiation of individual movements, such as running and turning, correlate with increases or depressions in DA of subsecond-to-second duration in both DS and VS. Interestingly, the fast DA fluctuations observed in the DS may couple directly to the $Ca^{2+}$-activity patterns of D1R- and D2R-expressing MSNs. In parallel to our findings, an increase in $Ca^{2+}$-activity was observed for D1R- and D2R-expressing MSNs at onset of a contraversive turn while a decrease was seen for an ipsilateral, turn (52). Indeed, this mirroring of the DA signal in $Ca^{2+}$ dynamics of DA target neurons indicates that DA signaling in the DS on a hundreds-of-millisecond scale is critical for coordination of moment-to-moment movements controlled by the basal ganglia. Recently, ipsiversive depressions and contraversive increases were also observed at onset of turns in the DS by use of the genetically encoded sensor $GRAB_{DA}$ (53); however, the

changes observed lasted several seconds after onset, which may be attributed to the slower off-rate kinetics of this sensor (53, 54).

While the DS signal correlated with movement on a fast timescale, syllable initiation rather coincided for the VS signal with second-long changes and slow fluctuations. Specifically, we observed changes in DS signal right at movement onset, whereas VS signal mainly increased immediately after initiation of high-velocity movements. This was observed in combination with the lateral pattern in DS during running turns, suggesting an element of modularity in the system. Moreover, our cross-correlation analysis supported considerable intrastriatal predictive power of the DA signal; hence, DA appears to be released in a coordinated and differential fashion to integrate the distinct functions of striatal subregions on subsecond-to-second time scales. Importantly, the data lend support to suggested interdependency proposed by Kelly & Moore in 1976 between VS and DS for executing motor behaviors such as turning (55). It may also be considered to what degree our findings may relate to recent observations indicating wave-like DA activation patterns across striatal regions (56). However, we cannot, at this stage, say how the cooperativity between DS and VS is coordinated, or whether it is direct or indirect. We should note that we cannot, based on the current data, say whether the correlation between DS and VS only exist cross-hemispherically, as space constraints did not allow simultaneous measurements in DS and VS of the same hemisphere. It will also be interesting in future studies to investigate DA dynamics in further striatal subregions, i.e., assessing how the DA signal might vary across the DS from the dorsolateral to the dorsomedial part.

Upon blockage of DA reuptake by exposure to cocaine, both regions exhibited massive elevation in the DA signal on a slow time scale. For VS, this was accompanied by an almost complete loss of correlation to behavioral syllables, while the correlation between DS DA and syllables increased. This differential response was reflected in a remarkable decoupling of the dorsoventral striatal coordination as shown in the cross-correlation analysis. Combined, this might speak in favor of the previously proposed gate-like role of DA in VS (57), where the moment-to-moment DA levels constitute a signal to exert distinct behaviors under normal circumstances. When DA is artificially elevated by cocaine, it seems therefore that DA signaling in DS takes control. However, in addition to increases in basal DA, the rapid DS fluctuations no longer carried salient information based on an unchanged variance of the derivative across intensities, yet these apparently random changes in DS DA still correlated with syllables. Curiously, this was accompanied by a more disordered sequencing of syllables as apparent from the increase in transition entropy, despite the general upregulation of the most frequent syllables. We speculate that the cooccurrence of these two phenomena represents a direct link between DA signaling in DS and the stringing together or structuring of actions on a moment-to-moment basis; that is, DS DA might modulate overall behavioral selection on a moment-to-moment basis but does not select specific actions. Taken together, the cocaine data both support a key role of DAT in governing discrete DA dynamics in DS and VS, and emphasize distinct functional roles of DA in DS and VS, that are directly reflected in differences in how information is encoded by the two regions. We should note, however, that cocaine also inhibits uptake of serotonin and norepinephrine (45), which could interfere with the results obtained.

In summary, we exploit the DA sensor dLight1.3b to reveal highly differential but cooperative DA dynamics in the DS and VS, that can be directly linked to discrete behavioral actions on time scales from hundreds of milliseconds to minutes. We find evidence of diverging modes of informational encoding that implores the need to consider regional differences when studying DA signaling. Moreover, we demonstrate the strength of a machine learning-based data analysis pipeline, which can be readily applied to studies across brain regions and neurotransmitters with genetically encoded biosensors. Indeed, this might represent a critical framework for future efforts aimed at gaining better insights into the complex pathobiology of neurological and psychiatric diseases involving dopamine and other important neurotransmitters.

## Materials and Methods

Detailed *Materials and Methods* with description of mice, DNA and AAV constructs, stereotaxic injections and implants, behavioral testing, immunohistochemistry, fiber photometry recordings and analysis, drugs, wavelet transform, mouse tracking and syllable analysis, information analysis, and statistics are included in *SI Appendix*.

**Mice.** All procedures were carried out in accordance with the institutional regulations and guidelines of University of Copenhagen and the Danish Animal Experimentation Inspectorate (License number: 2017-15-0201-01160). Male Th-Cre mice (58) were bred in house with female WT C57Bl6N mice supplied from Charles River as breeders.

**Stereotaxic Injections and Implants.** Mice were anesthetized using isoflurane and placed in a Neurostar Stereotaxic Robot frame before injection of AAV constructs. For implant sites (DS and VS) used for subsequent fiber photometry, 300 nL AAV9-hSyn-dLight1.3b-WPREpA or AAV9-hSyn-EGFP-WPREpA at a titer of $3.0*10^{12}$ viral genomes/mL was injected at the target coordinate of the implant, and 100 nL was injected 200 µm both below and above the target coordinate (VS: AP: 1.54 mm, ML: -0.80 mm, DV: -4.30 mm; DS: AP: 1.18 mm, ML. 1.70 mm, DV: -3.00 mm)**.** For DREADD injections in the VTA, 500 nL AAV8-hSyn-hM4Di-mCherry-WPREpA was injected bilaterally at coordinates AP: −3.20 mm, ML: ± 0.50 mm, DV: −4.50 mm and for SNc 300 nL was injected bilaterally at AP: −3.16 mm, ML: −1.60 mm, DV: −4.2 mm and 200 nL was injected bilaterally at AP: −3.00 mm, ML: ±1.20 mm, DV: −4.5 mm. After injections, a 200 µm ø 0.37NA 1.25 mm metal ferrule optic cannula (Doric Lenses) was slowly inserted at the target coordinate. Mice were tested at least 3 wk after surgery.

**Behavioral Testing.** Mice were tested and recorded in custom-made white arenas from the local technical workshop. For tests of responses to a novel environment and female soiled bedding, an arena measuring 45 × 30 × 15 cm with a 15-cm divider in the middle of one end and removable doors. For testing of self-paced exploratory activity before and after cocaine, we used an arena measuring 50 × 50 × 40 cm that the mice previously had been exposed to two to three times. Mice were recorded from above using an ELP KL36IR 1080P Full HD Webcam at 30 frames pr. second. For each test, hM4Di-injected mice were tested in a cross-over design with CNO and vehicle administration. Half of the mice received CNO on the first test day and vehicle on the second, while the other half received vehicle on test day one and CNO on the second test day. Data were pooled for both test days.

**Fiber Photometry Recordings.** Fiber photometric recordings of dLight1.3b fluorescence was measured using primarily the Neurophotometrics FP3001. Some control experiments were performed on the Neurophotometrics FP3002 as the setup was updated during the course of the experiments. For all experiments, except the ones using female bedding, two mice were recorded simultaneously in separate arenas using a 3-m long multibranching fiber optic patch cord (Doric Lenses, 200 µm, NA 0.37) attached to the implanted optic cannulas using bronze mating sleeves (Thorlabs ADAL 4-5). Fiber photometry recordings were performed using the open-source software Bonsai (59). Light power of the 470-nm channel was ~25 µW measured at the patch cord tip at constant illumination (slight differences between different fibers of the patch cord). The power of the isosbestic 415 nm channel was ~18 µW measured at the patch cord tip at constant illumination.

**Fiber Photometry Analysis.** Raw intensity measurements were preprocessed by subtracting a technical baseline from recordings with light-impermeable caps followed by the isosbestic 415-nm reference to account for artifacts. For cocaine trials, a linear regression to correct for photobleaching was fitted to data from before vehicle injection and the last 10 min of the trial and applied across the series. The resulting signal was converted to ΔF/F0 by dividing with the reference signal. For comparison across mice a running z-score (zF) was computed using the mean and SD from the 5 min preceding injection (*SI Appendix*, Fig. S1*C*).

**Mouse Tracking and Syllable Analysis.** Using top-down recorded videos, mice were tracked using DeepLabCut v2.2rc3 (43). Coordinates for snout, shoulders, hips, and base-of-tail were extracted and used to segregate movements into individual syllables using B-SOiD v2.0 (44). 67 clusters were identified, several empty, and due to intermouse variation and infrequent use, only 20 syllables were analyzed in the study.

**Statistical Analysis.** Choice of statistical analysis is presented in the legends associated with each figure, and multiple comparisons is corrected for using either the Tukey HSD procedure for post hoc ANOVA testing, Bonferroni–Holm when *t* tests are performed, or Benjamini–Hochberg false discovery rate for the information analysis due to the nonnegative correlation between tests. All *n* values are individual mice.

**Data, Materials, and Software Availability.** Fiber photometry raw data and code for analysis data have been deposited in https://github.com/GetherLab/In-vivo-dopamine-dynamics (10.5281/zenodo.7401221). Raw data and associated codes are available at https://github.com/GetherLab/In-vivo-dopamine-dynamics (60). Data from individual figures are found in Supporting Information. Further details of the analysis are available from the corresponding author upon request.

**ACKNOWLEDGMENTS.** We thank Anette Dencker Kaas for excellent technical assistance. The work was supported by the Lundbeck Foundation grants R266-2017-4331 (U.G.), R276-2018-792 (U.G.), R230-2016-3154 (M.D.L.), R181-2014-3090 (F.H.), R303-2018-3540 (F.H.) and R231-2016-2481-5 (A.T.S.), Independent Research Fund Denmark – Medical Sciences (U.G. 7016-00325B).

Author affiliations: [a]Department of Neuroscience, Faculty of Health and Medical Sciences, University of Copenhagen, DK-2200 Copenhagen, Denmark; [b]Departments of Biochemistry and Molecular Medicine, School of Medicine, University of California, Davis, CA, 95616; and [c]Department of Bioinformatics, H Lundbeck A/S, DK-2500 Valby, Denmark

Author contributions: S.H.J., A.L.E., A.T.S. and U.G. designed research; S.H.J., A.L.E. and L.P.P. performed research; L.T. and J.K.D. contributed new reagents/analytical tools; S.H.J., A.L.E., M.D.L., K.L.M., J.K.D., F.H., A.T.S., and U.G. analyzed data; and S.H.J., A.L.E., and U.G. wrote the paper.

1. N. X. Tritsch, B. L. Sabatini, Dopaminergic modulation of synaptic transmission in cortex and striatum. *Neuron* **76**, 33–50 (2012).
2. S. D. Iversen, L. L. Iversen, Dopamine: 50 years in perspective. *Trends Neurosci.* **30**, 188–193 (2007).
3. W. Schultz, Multiple dopamine functions at different time courses. *Annu. Rev. Neurosci.* **30**, 259–288 (2007).
4. A. Klaus, J. Alves da Silva, R. M. Costa, What, if, and when to move: Basal ganglia circuits and self-paced action initiation. *Annu. Rev. Neurosci.* **42**, 459–483 (2019).
5. A. H. Runegaard *et al.*, Modulating dopamine signaling and behavior with chemogenetics: Concepts, progress, and challenges. *Pharmacol. Rev.* **71**, 123–156 (2019).
6. J. D. Berke, What does dopamine mean? *Nat. Neurosci.* **21**, 787–793 (2018).
7. L. F. Agnati, B. Bjelke, K. Fuxe, Volume versus wiring transmission in the brain: A new theoretical frame for neuropsychopharmacology. *Med. Res. Rev.* **15**, 33–45 (1995).
8. D. O. Borroto-Escuela *et al.*, Brain dopamine transmission in health and Parkinson's disease: Modulation of synaptic transmission and plasticity through volume transmission and dopamine heteroreceptors. *Front. Synaptic. Neurosci.* **10**, 20 (2018).
9. C. Liu, P. Goel, P. S. Kaeser, Spatial and temporal scales of dopamine transmission. *Nat. Rev. Neurosci.* **22**, 345–358 (2021).
10. J. J. Day, M. F. Roitman, R. M. Wightman, R. M. Carelli, Associative learning mediates dynamic shifts in dopamine signaling in the nucleus accumbens. *Nat. Neurosci.* **10**, 1020–1028 (2007).
11. M. W. Howe, D. A. Dombeck, Rapid signalling in distinct dopaminergic axons during locomotion and reward. *Nature* **535**, 505–510 (2016).
12. M. G. Kutlu *et al.*, Dopamine release in the nucleus accumbens core signals perceived saliency. *Curr. Biol.* **31**, 4748–4761.e4748 (2021).
13. A. Mohebi *et al.*, Dissociable dopamine dynamics for learning and motivation. *Nature* **570**, 65–70 (2019).
14. J. A. da Silva, F. Tecuapetla, V. Paixao, R. M. Costa, Dopamine neuron activity before action initiation gates and invigorates future movements. *Nature* **554**, 244–248 (2018).
15. A. A. Hamid *et al.*, Mesolimbic dopamine signals the value of work. *Nat. Neurosci.* **19**, 117–126 (2016).
16. A. A. Grace, Dysregulation of the dopamine system in the pathophysiology of schizophrenia and depression. *Nat. Rev. Neurosci.* **17**, 524–532 (2016).
17. R. A. Wise, M. A. Robble, Dopamine and addiction. *Annu. Rev. Psychol.* **71**, 79–106 (2020).
18. B. R. Bloem, M. S. Okun, C. Klein, Parkinson's disease. *Lancet* **397**, 2284–2303 (2021).
19. A. Jaquins-Gerstl, A. C. Michael, A review of the effects of FSCV and microdialysis measurements on dopamine release in the surrounding tissue. *Analyst* **140**, 3696–3708 (2015).
20. M. R. Post, D. Sulzer, The chemical tools for imaging dopamine release. *Cell Chem. Biol.* **28**, 748–764 (2021).
21. M. Ganesana, S. T. Lee, Y. Wang, B. J. Venton, Analytical techniques in neuroscience: Recent advances in imaging, separation, and electrochemical methods. *Anal. Chem.* **89**, 314–341 (2017).
22. A. A. Grace, B. S. Bunney, The control of firing pattern in nigral dopamine neurons: burst firing. *J. Neurosci.* **4**, 2877–2890 (1984).
23. D. Sulzer, S. J. Cragg, M. E. Rice, Striatal dopamine neurotransmission: Regulation of release and uptake. *Basal Ganglia* **6**, 123–148 (2016).
24. C. A. Paladini, J. Roeper, Generating bursts (and pauses) in the dopamine midbrain neurons. *Neuroscience* **282**, 109–121 (2014).
25. P. D. Dodson *et al.*, Representation of spontaneous movement by dopaminergic neurons is cell-type selective and disrupted in parkinsonism. *Proc. Natl. Acad. Sci. U.S.A.* **113**, E2180–E2188 (2016).
26. J. W. Barter *et al.*, Beyond reward prediction errors: The role of dopamine in movement kinematics. *Front. Integr. Neurosci.* **9**, 39 (2015).
27. B. Panigrahi *et al.*, Dopamine is required for the neural representation and control of movement vigor. *Cell* **162**, 1418–1430 (2015).
28. A. Bova *et al.*, Precisely timed dopamine signals establish distinct kinematic representations of skilled movements. *Elife* **9**, e61591 (2020).
29. T. Patriarchi *et al.*, Ultrafast neuronal imaging of dopamine dynamics with designed genetically encoded sensors. *Science* **360**, eaat4422 (2018).
30. F. Sun *et al.*, A genetically encoded fluorescent sensor enables rapid and specific detection of dopamine in flies, fish, and mice. *Cell* **174**, 481–496.e419 (2018).
31. H. Dong *et al.*, Dorsal striatum dopamine levels fluctuate across the sleep-wake cycle and respond to salient stimuli in mice. *Front. Neurosci.* **13**, 242 (2019).
32. P. Gonzalez-Rodriguez *et al.*, Disruption of mitochondrial complex I induces progressive parkinsonism. *Nature* **599**, 650–656 (2021).
33. E. S. Calipari, K. N. Huggins, T. A. Mathews, S. R. Jones, Conserved dorsal-ventral gradient of dopamine release and uptake rate in mice, rats and rhesus macaques. *Neurochem. Int.* **61**, 986–991 (2012).
34. A. A. Grace, Phasic versus tonic dopamine release and the modulation of dopamine system responsivity: A hypothesis for the etiology of schizophrenia. *Neuroscience* **41**, 1–24 (1991).
35. J. K. Dreyer, K. F. Herrik, R. W. Berg, J. D. Hounsgaard, Influence of phasic and tonic dopamine release on receptor activation. *J. Neurosci.* **30**, 14273–14283 (2010).
36. J. K. Dreyer, J. Hounsgaard, Mathematical model of dopamine autoreceptors and uptake inhibitors and their influence on tonic and phasic dopamine signaling. *J. Neurophysiol.* **109**, 171–182 (2013).
37. J. K. Dreyer, C. M. Vander Weele, V. Lovic, B. J. Aragona, Functionally distinct dopamine signals in nucleus accumbens core and shell in the freely moving rat. *J. Neurosci.* **36**, 98–112 (2016).
38. Y. Beny-Shefer *et al.*, Nucleus accumbens dopamine signaling regulates sexual preference for females in male mice. *Cell Rep.* **21**, 3079–3088 (2017).
39. A. H. Runegaard *et al.*, Locomotor- and reward-enhancing effects of cocaine are differentially regulated by chemogenetic stimulation of gi-signaling in dopaminergic neurons. *eNeuro* **5**, ENEURO.0345-17.2018 (2018).
40. Y. L. Hurd, Z. B. Pristupa, M. M. Herman, H. B. Niznik, J. E. Kleinman, The dopamine transporter and dopamine D2 receptor messenger RNAs are differentially expressed in limbic- and motor-related subpopulations of human mesencephalic neurons. *Neuroscience* **63**, 357–362 (1994).
41. S. J. Cragg, S. A. Greenfield, Differential autoreceptor control of somatodendritic and axon terminal dopamine release in substantia nigra, ventral tegmental area, and striatum. *J. Neurosci.* **17**, 5738–5746 (1997).
42. J. E. Markowitz *et al.*, The striatum organizes 3D behavior via moment-to-moment action selection. *Cell* **174**, 44–58.e17 (2018).
43. A. Mathis *et al.*, DeepLabCut: markerless pose estimation of user-defined body parts with deep learning. *Nat. Neurosci.* **21**, 1281–1289 (2018).
44. A. I. Hsu, E. A. Yttri, B-SOiD, an open-source unsupervised algorithm for identification and fast prediction of behaviors. *Nat. Commun.* **12**, 5188 (2021).
45. A. S. Kristensen *et al.*, SLC6 neurotransmitter transporters: Structure, function, and regulation. *Pharmacol. Rev.* **63**, 585–640 (2011).
46. I. Tsutsui-Kimura *et al.*, Distinct temporal difference error signals in dopamine axons in three regions of the striatum in a decision-making task. *Elife* **9**, e62390 (2020).
47. N. F. Parker *et al.*, Reward and choice encoding in terminals of midbrain dopamine neurons depends on striatal target. *Nat. Neurosci.* **19**, 845–854 (2016).
48. W. van Elzelingen *et al.*, A unidirectional but not uniform striatal landscape of dopamine signaling for motivational stimuli. *Proc. Natl. Acad. Sci. U.S.A.* **119**, e2117270119 (2022).
49. J. Grenhoff, L. Ugedo, T. H. Svensson, Firing patterns of midbrain dopamine neurons: differences between A9 and A10 cells. *Acta. Physiol. Scand.* **134**, 127–132 (1988).
50. D. Clark, L. A. Chiodo, Electrophysiological and pharmacological characterization of identified nigrostriatal and mesoaccumbens dopamine neurons in the rat. *Synapse* **2**, 474–485 (1988).
51. M. Marinelli, J. E. McCutcheon, Heterogeneity of dopamine neuron activity across traits and states. *Neuroscience* **282**, 176–197 (2014).
52. F. Tecuapetla, S. Matias, G. P. Dugue, Z. F. Mainen, R. M. Costa, Balanced activity in basal ganglia projection pathways is critical for contraversive movements. *Nat. Commun.* **5**, 4315 (2014).
53. C. Liu *et al.*, An action potential initiation mechanism in distal axons for the control of dopamine release. *Science* **375**, 1378–1385 (2022).
54. C. Klein Herenbrink *et al.*, Multimodal detection of dopamine by sniffer cells expressing genetically encoded fluorescent sensors. *Commun. Biol.* **5**, 578 (2022).
55. P. H. Kelly, K. E. Moore, Mesolimbic dopaminergic neurones in the rotational model of nigrostriatal function. *Nature* **263**, 695–696 (1976).
56. A. A. Hamid, M. J. Frank, C. I. Moore, Wave-like dopamine dynamics as a mechanism for spatiotemporal credit assignment. *Cell* **184**, 2733–2749.e2716 (2021).
57. S. B. Floresco, The nucleus accumbens: An interface between cognition, emotion, and action. *Annu. Rev. Psychol.* **66**, 25–52 (2015).
58. J. M. Savitt, S. S. Jang, W. Mu, V. L. Dawson, T. M. Dawson, Bcl-x is required for proper development of the mouse substantia nigra. *J. Neurosci.* **25**, 6721–6728 (2005).
59. G. Lopes *et al.*, Bonsai: An event-based framework for processing and controlling data streams. *Front. Neuroinform.* **9**, 7 (2015).
60. A.L. Ejdrup, S.H. Jørgensen, U. Gether, Github page Gether Lab. *Repository: In-vivo-dopamine-dynamics.* https://github.com/GetherLab/In-vivo-dopamine-dynamics 5 December 2022.